Hindawi
International Journal of Aerospace Engineering
Volume 2019, Article ID 5737212, 15 pages
https://doi.org/10.1155/2019/5737212

Research Article

Flight Dynamics Modeling and Dynamic Stability Analysis of Tilt-Rotor Aircraft

Ke Lu,[1,2] **Chunsheng Liu**,[1] **Chunhua Li**,[2] **and Renliang Chen**[3]

[1]*College of Automation Engineering, Nanjing University of Aeronautics and Astronautics, Nanjing, Jiangsu 210016, China*
[2]*Science and Technology on Rotorcraft Aeromechanics Laboratory, China Helicopter Research and Development Institute, Jingdezhen, Jiangxi 333001, China*
[3]*National Key Laboratory of Science and Technology on Rotorcraft Aeromechanics, Nanjing University of Aeronautics and Astronautics, Nanjing, Jiangsu 210016, China*

Correspondence should be addressed to Ke Lu; looknuaa@163.com

Received 16 December 2018; Revised 17 March 2019; Accepted 22 April 2019; Published 14 August 2019

Academic Editor: Youmin Zhang

The tilt-rotor aircraft has often been proposed as a means to increase the maximum speed of the conventional helicopter. The tilt-rotor aircraft consists of three primary flight modes that are the helicopter flight mode in low forward speed flight, airplane flight mode in high forward speed flight, and conversion flight mode. The aim of this paper is to develop a nonlinear flight dynamics mathematical modeling method of tilt-rotor aircraft and investigate the dynamic stability characteristics of tilt-rotor aircraft. First, a nonlinear tilt-rotor aircraft flight dynamics model is developed. The trim and linearized results are present to verify the model. Then, using a numerical differentiation technique, the dynamic stability of the tilt-rotor aircraft is assessed. The results show that the flight speed and nacelle angle would affect the magnitude and the trend of the aerodynamic derivatives. The damping of the pitch short period mode and the Dutch roll mode is insensitive to flight speed while they could be affected by nacelle angle. In all flight modes, as flight speed increases, the natural modes become more stable.

1. Introduction

The maximum speed of a conventional helicopter is restricted due to aerodynamic limitations, installed engine power, and airframe drag [1]. The problems associated with installed engine power and airframe drag could be minimized through careful design, but the main factor limiting the maximum speed of the helicopter is retreating blade stall. To achieve high-speed flight, tilt-rotor is a good way to achieve it. Tilt-rotor aircraft combines the vertical lift ability of helicopters and the speed and range of fixed-wing airplanes and has found wide applications in both military and civil fields. As shown in Figure 1, tilt-rotor aircraft has three flight modes: helicopter mode, conversion mode, and airplane mode. In helicopter mode, two rotors are oriented in the same way as a conventional helicopter to provide the lifting force in the hover. As the vehicle moves into forward flight, the two rotors are progressively tilted forward so that the thrust from the two rotors provide a propulsive force. Eventually, the aircraft reaches airplane mode, where it resembles a fixed-wing aircraft with the two rotors becoming two propotors with the wing providing the lifting force.

The XV-15 was a successful tilt-rotor aircraft technology demonstrator. Reference [2] gave a brief history of the XV-15 tilt-rotor aircraft. It also introduced the main feature of the tilt-rotor aircraft. To support the analysis of flight dynamics, pilot-in-the-loop simulation, and flight control design, the Generic Tilt-rotor Simulation (GTRS) was developed [3]. The simulation model is mainly based on 1/5 model scale wind-tunnel data. The detailed lookup tables include the effects of nacelle angle, angle of attack, sideslip, flap deflections, Mach number, etc., on aerodynamic coefficients and contain correction factors to the dynamic response of the aircraft [4]. Reference [5] provides comparisons between the models developed for the XV-15 and flight data. Flight dynamics models of the XV-15 were also obtained from frequency domain identification technology [6, 7]. Kleinhesselink developed a simple open-source model of a tilt-rotor

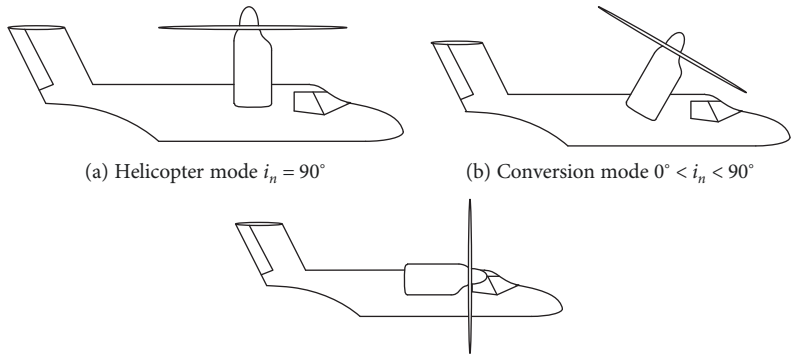

(a) Helicopter mode $i_n = 90^\circ$ (b) Conversion mode $0^\circ < i_n < 90^\circ$

(c) Airplane mode $i_n = 0^\circ$

Figure 1: Tilt-rotor aircraft three flight modes.

using the basic equations of motion [8]. The model focused on stability and control aspects of the XV-15 aircraft and did not add the corrections. NASA has developed a "Large Civil Tilt-rotor" concept. The configuration weighs around 100,000 lbs and has a 107 ft wingspan and two tilting nacelles supporting 65 ft diameter rotors [9]. In order to analyze this kind of tilt-rotor aircraft, a high-order rotorcraft mathematical model is developed [10]. Piloted studies were designed to test hover and low-speed handling qualities and control system architectures of "Large Civil Tilt-rotor" [11–13]. It is clear that there are some literature regarding the tilt-rotor aircraft; however, the majority of these studies focus on flight dynamics modeling and handling quality evaluation. The dynamic stability of the tilt-rotor aircraft is less investigated, in particular, the variation trend of the stability derivatives in three flight modes. To this end, the aim of this paper is to examine the stability derivatives of tilt-rotor aircraft in three flight modes. In order to analyze the variation trend of stability derivatives, the contributions of each aerodynamic component to the stability derivatives in the different nacelle angles are investigated. In addition, the tilt-rotor aircraft flight behavior can be considered to comprise a linear combination of natural modes. The frequency, damping, and distribution of each natural mode are investigated to understand how the tilt-rotor aircraft responds following a small perturbation to a vehicle state.

This paper is organized as follows. In Section 2, XV-15 tilt-rotor aircraft flight dynamics model for dynamic stability analysis is developed. Peters-He finite-state inflow model is used to represent the induced inflow distribution at the rotor plane. Rotor-wing-empennage interaction is modeled similar to GTRS [3]. In addition, model validation is presented. In Section 3, the stability derivatives are analyzed. We focus on the variation trend of the stability derivatives in three flight modes, and then, natural modes are presented. Finally, conclusions are summarized in Section 4.

2. Mathematical Model

In this section, a nonlinear flight dynamics model of the tilt-rotor aircraft is established.

2.1. Model Description. XV-15 tilt-rotor aircraft is chosen for this analysis. The basic parameters are shown in Table 1. The detailed parameters could be found in reference [3].

2.1.1. Rotor Model. The rotor model is the most important part of the tilt-rotor aircraft model, and it is also the most complex component of the model due to the flapping motion and solution of induced velocity. As shown in Figure 2, flapping motion induces velocity and rotor aerodynamic force is coupled.

The blade-root collective pitch is given by

$$\theta_b = \theta_0 - \theta_{1c} \cos(\psi) - \theta_{1s} \sin(\psi) + \theta_t(\bar{r}) - K_p \beta. \quad (1)$$

The XV-15 tilt-rotor has two 3-bladed gimbaled rotors. The pitch-flap coupling delta-three angle is 15 deg, which means decreasing the blade pitch for a flap increase. The feedback gain for pitch-coupling is given by [14]

$$K_p = \tan \delta_3. \quad (2)$$

The motion of the gimbaled hub relative to the shaft could be described by two degrees of freedom: the lateral tilt and longitudinal tilt angles. These two degrees of freedom correspond to the tip-path-plane tilt of an articulated rotor [14]. In a sense, the gimbaled hub system is a special case of an articulated system. In view of this, the rotor system is treated as an articulated system for flight dynamics modeling.

The hinge offset and flapping hinge restraint parameters are given in Table 1.

Figure 3 shows the flapping motion of rotor blade. The flapping equation is given by

$$I_b\left(\ddot{\beta} + \Omega^2 \beta\right) + K_\beta\left(\beta - \beta_p\right) = \int_0^R r F_z dr. \quad (3)$$

Consider incompressible, potential flow about a rotor, the induced inflow distribution at the rotor plane could be

Table 1: Basic parameters of XV-15 tilt-rotor.

Parameters value	
Weight (m)	5897 kg
Rotor radius (R)	3.81 m
Blade number (N_b)	3×2
Blade twist (θ_t)	-41°
Rotor speed (Ω)	589 rpm (helicopter mode) 517 rpm (airplane mode)
Lock number (γ)	3.83
Solidity (σ)	0.089
Pitch-flap coupling angle (δ_3)	15 deg
Flapping hinge restraint (K_β)	17476 Nm/rad
Flap moment of inertia (I_β)	139 kg·m^2
Nacelle length (d)	1.4 m
Wing area (S_w)	16.82 m^2
Horizontal tail areas (S_{ht})	4.67 m^2
Vertical tail areas (S_{vt})	2.35 m^2

represented in terms of a set of harmonic and radial shape functions [15].

$$v_i(\bar{r}, \psi, t) = \sum_{m=0}^{\infty} \sum_{n=m+1,m+3,\cdots}^{\infty} \phi_n^m(\bar{r}) \left[\alpha_n^m(t) \cos(m\psi) + \beta_n^m(t) \sin(m\psi)\right], \tag{4}$$

with

$$\phi_n^m(\bar{r}) = \sqrt{(2n+1)H_n^m} \sum_{q=m,m+2,\cdots}^{n-1} \bar{r}^q \frac{(-1)^{(q-m)/2}(n+q)!!}{(q-m)!!(q+m)!!(n-q-1)!!},$$
$$H_n^m = \frac{(n+m-1)!!(n-m-1)!!}{(n+m)!!(n-m)!!}. \tag{5}$$

For engineering applications, truncations are required. The rule is to make the induced flow harmonic match the highest frequency we care about [16]. In this study, the XV-15 tilt-rotor aircraft has two three-bladed rotors, so the inflow is truncated after the third harmonic. The highest power of radial variation is $\bar{r}^4$. This would be 13 inflow states in total for each rotor.

2.1.2. Wing Model. The wing aerodynamic coefficients are defined as functions of angle of attack, nacelle angle, and flap setting. Because part of the wing is disturbed by the rotor wake, it is necessary to take into account the rotor's wake interference in wing modeling. The wing is divided into slipstream and freestream parts. The area of the wing influenced by rotor wake is given by [17]

$$S_{wss} = \begin{cases} 0, & i_n < 60 \text{ deg or } u \geq u_{cr}, \\ S_{ss\ \max} \dfrac{u_{cr} - u}{u_{cr}} \left[\sin(0.0242 i_n) + \cos(0.0543 i_n)\right], & \text{else}, \end{cases} \tag{6}$$

where $S_{ss\ \max} = 2\eta_{ss} R c_w$, $\eta_{ss} < 1$, R is the rotor radius, c_w is the mean aerodynamic chord, and $u_{cr} = 40$ft/s is obtained by matching experimental data.

2.1.3. Empennage Model. Empennage aerodynamics are modeled similarly to the wing. The downwash at the empennage was assumed to be caused by the wing and the rotors [18]. The downwash due to the rotors was determined from wind tunnel and is given by [3]

$$v_{ih} = \left[c_0 + c_1 i_n + c_2 i_n (c_3 u + c_4 i_n + c_5)^2\right] v_{i0}, \tag{7}$$

where c_0, c_1, c_2, c_3, c_4, and c_5 are selected to match wind-tunnel data; v_{i0} means rotor-induced velocity.

The downwash angle at empennage due to the wing is also obtained from reference [3], which is a function of angle of attack at the inboard section of the wing, nacelle angle, and flap deflection. After considering the aerodynamic interference, the empennage aerodynamic coefficients are defined as functions of local angle of attack and the rudder/elevator setting.

2.1.4. Control Strategy. The XV-15 tilt-rotor aircraft uses both helicopter and airplane control strategies to control the aircraft. In helicopter flight mode, longitudinal cyclic, differential collective, and differential longitudinal cyclic are used to pitch, roll, yaw, and heave control, respectively. As the tilt-rotor aircraft converts from helicopter flight mode to airplane flight mode, the helicopter rotor control surfaces are washed out as function of nacelle angle and flight speed, which is given by

$$\begin{cases} \theta_{0,r} = \delta_{\text{coll}} - (\delta_{\text{lat}} - \delta_{\text{lat},n}) \partial\theta_0 / \partial\delta_{\text{lat}}, \\ \theta_{0,l} = \delta_{\text{coll}} + (\delta_{\text{lat}} - \delta_{\text{lat},n}) \partial\theta_0 / \partial\delta_{\text{lat}}, \\ \theta_{1s,r} = (\delta_{\text{long}} - \delta_{\text{long},n}) \partial\theta_{1s} / \partial\delta_{\text{long}} - (\delta_{\text{ped}} - \delta_{\text{ped},n}) \partial\theta_{1s} / \partial\delta_{\text{ped}}, \\ \theta_{1s,l} = (\delta_{\text{long}} - \delta_{\text{long},n}) \partial\theta_{1s} / \partial\delta_{\text{long}} + (\delta_{\text{ped}} - \delta_{\text{ped},n}) \partial\theta_{1s} / \partial\delta_{\text{ped}}. \end{cases} \tag{8}$$

The XV-15 tilt-rotor aircraft flight dynamics model could be given by

$$\dot{\mathbf{X}} = \mathbf{f}(\mathbf{X}, t) + \mathbf{g}(\mathbf{X}, t)\mathbf{u}. \tag{9}$$

The state variables are given in the form of a vector $\mathbf{X} \in R^{47\times1}$, which includes 26 rotor inflow states, 12 flapping motion states, and 9 aircraft states. $\mathbf{u} \in R^{4\times1}$ denotes a vector constituting the control inputs.

2.2. Mode Validation

2.2.1. Trim Result Validation. The trim calculation is to solve nonlinear differential equations, like equation (9), in order to find its equilibrium point. A trimmed flight condition is defined as one in which the resultant of the applied forces and moments is zero [19]. In this paper, the gradient descent method is used to solve the equilibrium point.

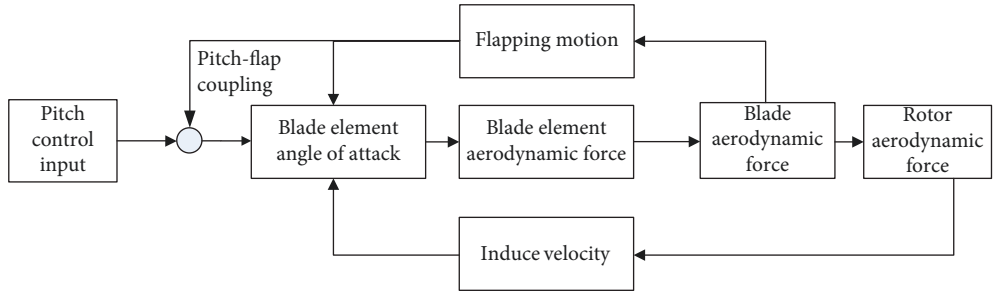

Figure 2: Rotor aerodynamic calculation diagram.

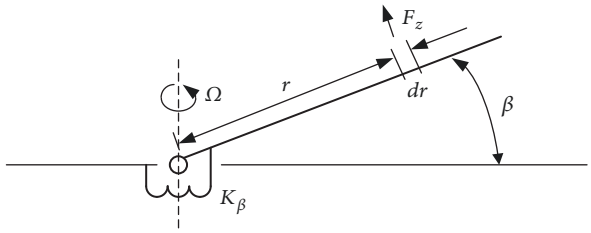

Figure 3: Rotor blade flapping motion.

In order to carry out trim validation, a comparison of the trim results with results from the GTRS is presented. Figures 4–7 show the comparison of helicopter mode, nacelle 60 deg conversion flight mode, nacelle 30 deg conversion flight mode, and airplane mode. The tilt-rotor aircraft mode appears to compare well with the GTRS mode in all flight modes. In helicopter mode, the variation trend of collective pitch is similar to the conventional helicopter. The collective pitch has the characteristic bucket profile as a function of flight speed. This is because the induced power decreases, and the parasite power increases as the speed increases. For pitch attitude, the tilt-rotor aircraft needs to nose down to produce the forward force in helicopter mode. In airplane mode, the function of the rotor turns into a propeller, providing only forward pull force to overcome fuselage drag. At this point, the wing is able to generate enough lift to overcome gravity. Due to the rotor working state in the axial flow, the collective pitch is much larger than that of the helicopter mode and the relationship between the collective pitch and the flight speed is almost linear. For pitch attitude, in airplane mode, with flight speed increasing, the wing needs smaller angle of attack.

2.2.2. Linearized Result Validation. With the application of a linearization algorithm, the rotor and inflow modes residualized out via quasistatic reduction, then the nonlinear equation can be reduced to the form of

$$\dot{\mathbf{x}} = \mathbf{A}\mathbf{x} + \mathbf{B}\mathbf{u}, \tag{10}$$

$$\mathbf{x} = [u, v, w, p, q, r, \phi, \theta, \psi], \tag{11}$$

$$\mathbf{u} = \left[\delta_{\text{coll}}, \delta_{\text{long}}, \delta_{\text{lat}}, \delta_{\text{ped}}\right]. \tag{12}$$

To linearize validation, a comparison of the eigenvalues for matrix A in equation (10) with results from the flight test and GTRS is shown in Tables 2 and 3. As shown Table 2, in helicopter mode, the characteristic of the eigenvalue distribution between calculation results in this paper and flight test is very similar. In helicopter mode, for phugoid and Dutch roll modes, this paper has a better comparison with flight test than reference [20]. In particular, for phugoid and Dutch roll modes, calculation results in this paper and reference [20] as well as flight test have given the conclusion of instability. The airplane mode eigenvalues are shown in Table 3. In general, the calculation results in this paper are closer to GTRS than those in reference [20], especially the prediction of short period modes. In airplane mode, all modes are stable.

In conclusion, the calculated values in this paper including trim and eigenvalues are in good agreement with those in the GTRS and flight test. In brief, the XV-15 tilt-rotor flight dynamics model is proved to be valid. So we have enough confidence in the following analysis results.

2.3. Longitudinal Static Stability. Longitudinal static stability is also called speed stability, which defined the relationship between the longitudinal stick and the flight speed. ADS-33E-PRF handling quality requirements require the longitudinal static stability to meet positive speed stability for cyclic control [21]. That is to say, push (pull) force on the longitudinal controller shall always be required to increase (decrease) speed.

In order to analyze the tilt-rotor aircraft speed stability, longitudinal stick trim results of all flight modes are drawn on a single graph, as shown Figure 8. The longitudinal stick in helicopter mode can be divided into three parts. The first part is the speed from hove to 20 knots. In this part, the speed stability is positive which means increasing forward stick with increasing airspeed. The second part is the speed from 20 knots to 40 knots. In this part, the speed stability is negative. That is to say, in order to gain airspeed, the pilot need to pull longitudinal stick back. The main reason of this phenomenon is aerodynamic interference of rotor wake and horizontal stabilizer. The third part is speed over 40 knots. In this part, since the rotor wake is outside the horizontal stabilizer, the speed stability becomes positive stability. In all conversion and airplane flight mode, the speed stability is always positive.

In order to study the speed stability in the conversion flight, a sample conversion path in conversion corridor is chosen. The conversion path begins at 80 knots in helicopter

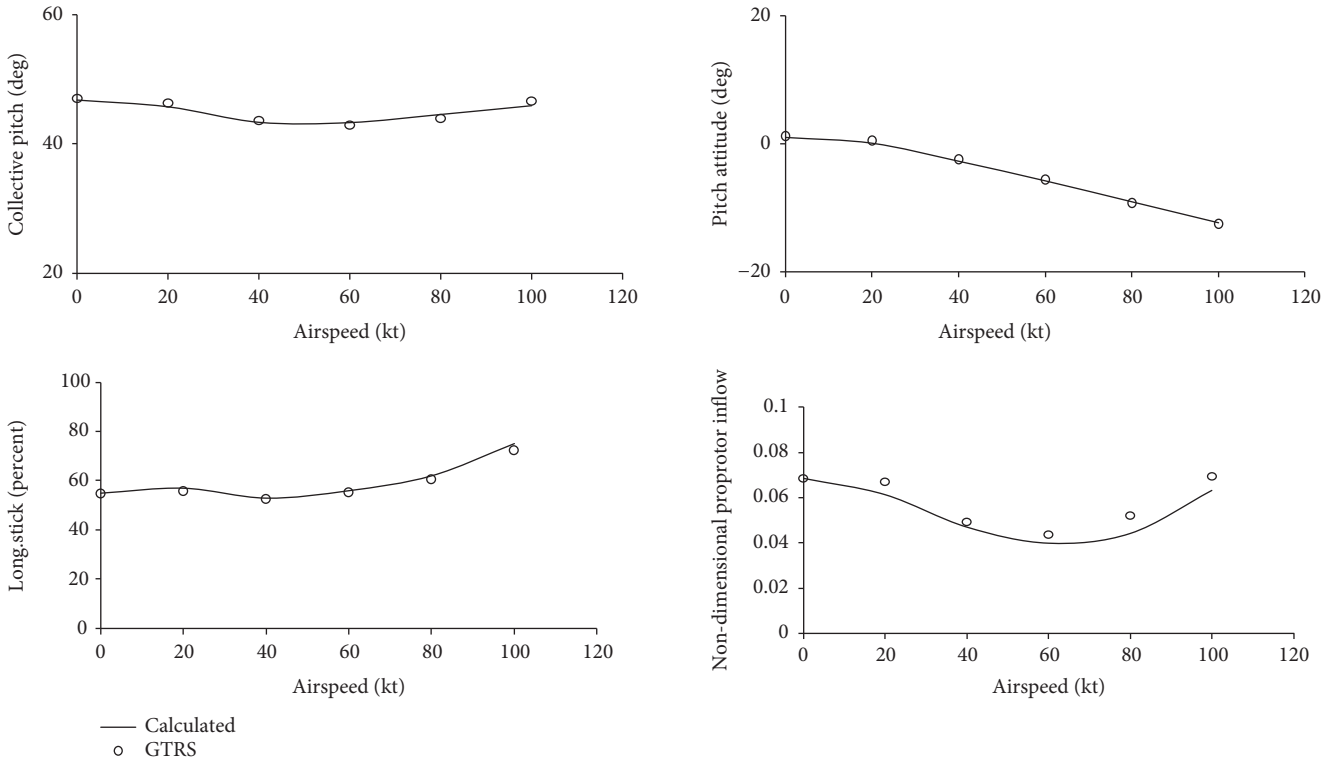

Figure 4: Trim results in helicopter mode.

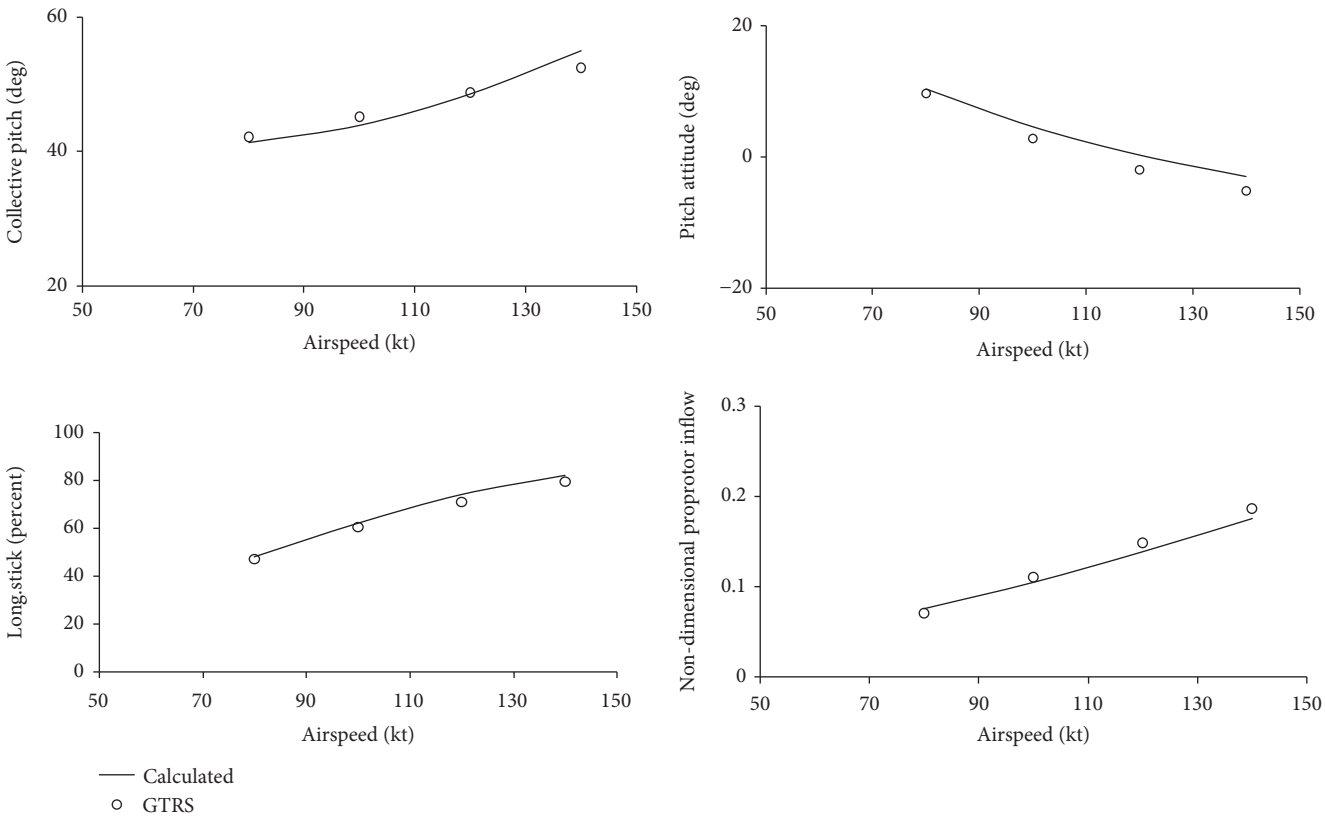

Figure 5: Trim results in nacelle 60 deg.

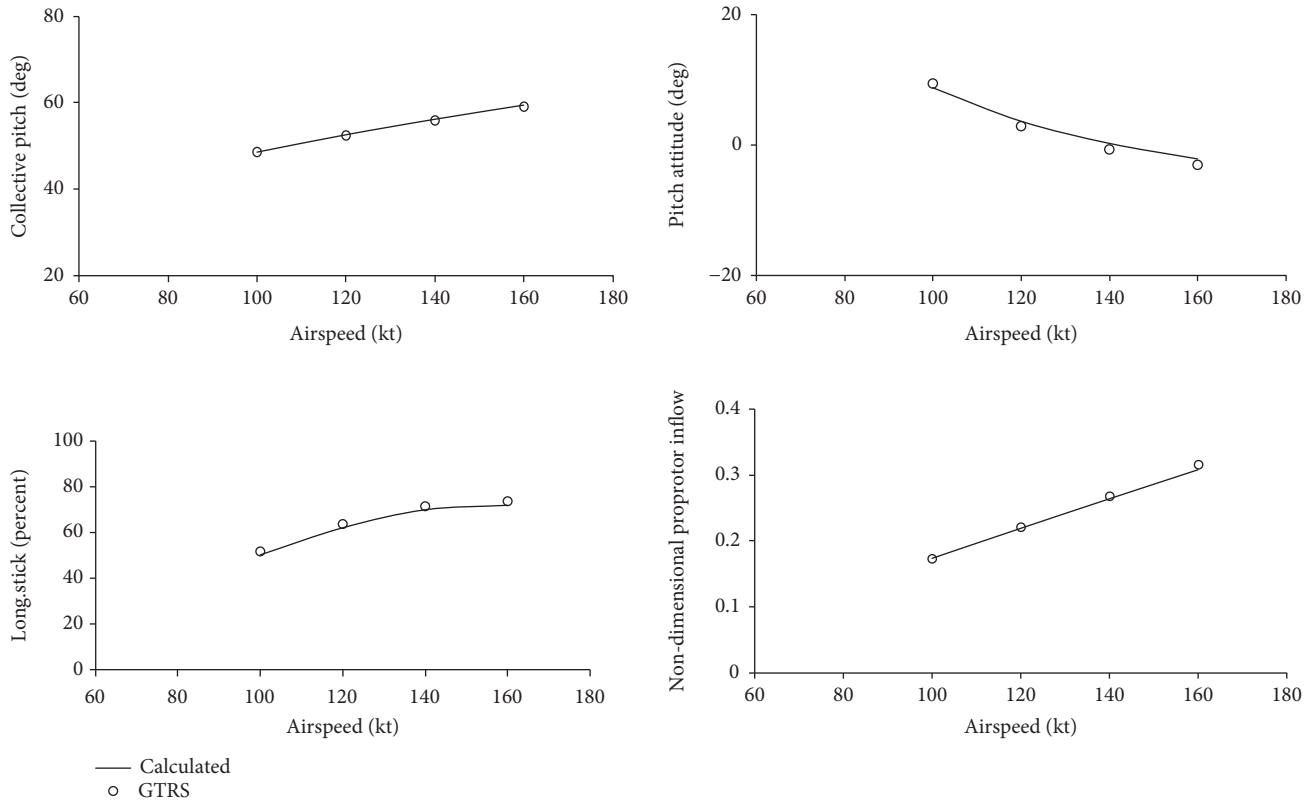

Figure 6: Trim results in nacelle 30 deg.

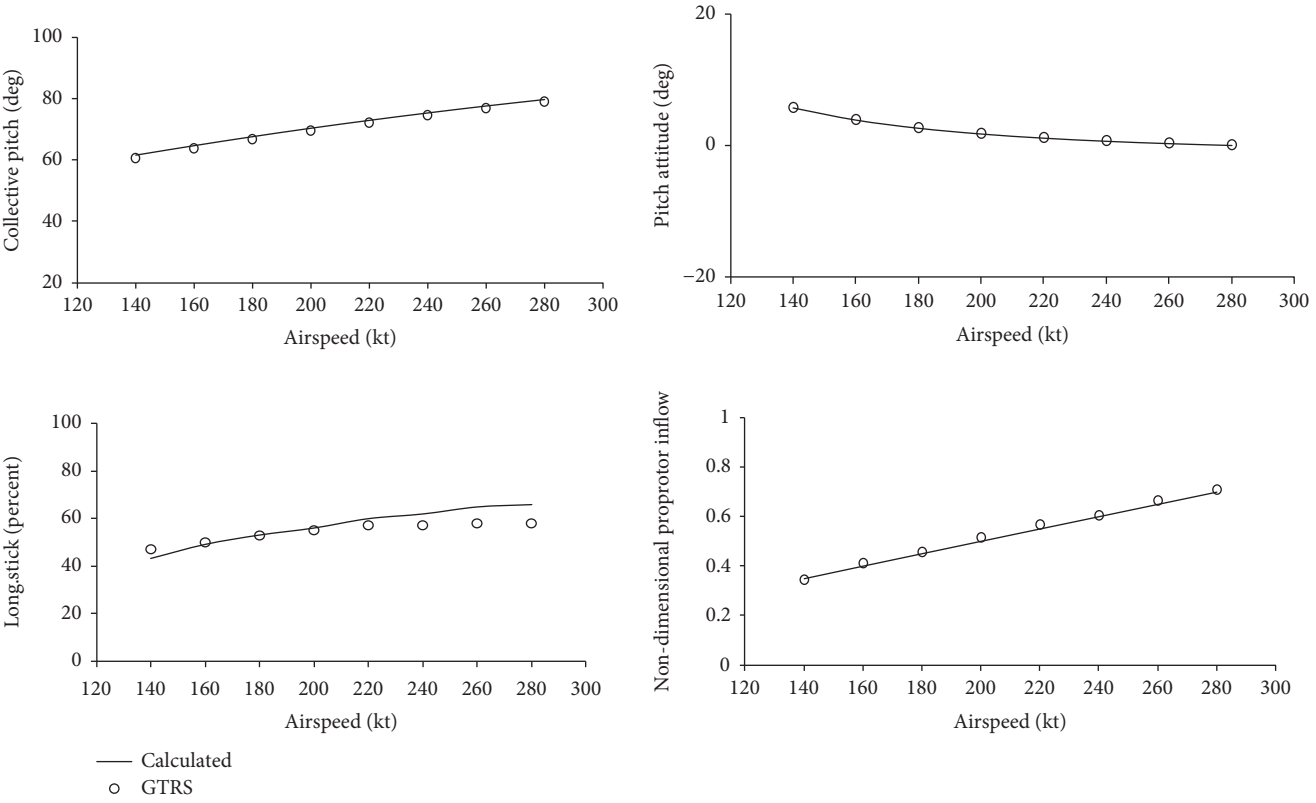

Figure 7: Trim results in airplane mode.

Table 2: Hover mode eigenvalue validation.

Hover mode	Natural mode	Calculated	Reference[20]	Flight test
Longitudinal	Phugoid	$0.2981 \pm 0.7555i$	$0.1772 \pm 0.4302i$	$0.2681 \pm 0.5132i$
	Pitch subsidence	-1.0	-0.5979	-1.32
	Heave subsidence	-0.17	-0.2086	-0.105
Lateral	Dutch roll	$0.1866 \pm 1.0826i$	$0.4723 \pm 0.8818i$	$0.1868 \pm 0.4061i$
	Spiral subsidence	-0.1609	-0.0728	-0.102
	Roll subsidence	-2.6539	−1.1247	-1.23

Table 3: Airplane mode $V = 200$ kt eigenvalue validation.

Hover mode	Natural mode	Calculated	Reference [20]	GTRS
Longitudinal	Phugoid	$-0.2111 \pm 0.2625i$	$-0.2387 \pm 0.2784i$	$-0.2115 \pm 0.1576i$
	Short-period pitch	$-1.7402 \pm 3.9172\,i$	$-1.3658 \pm 2.7521i$	$-1.6948 \pm 3.4555i$
Lateral	Dutch roll	$-0.6525 \pm 2.2092i$	$-0.6280 \pm 2.0094i$	$-0.4989 \pm 3.4555i$
	Spiral subsidence	-0.1384	-0.0497	-0.1226
	Roll subsidence	-0.7128	-0.9378	-1.0649

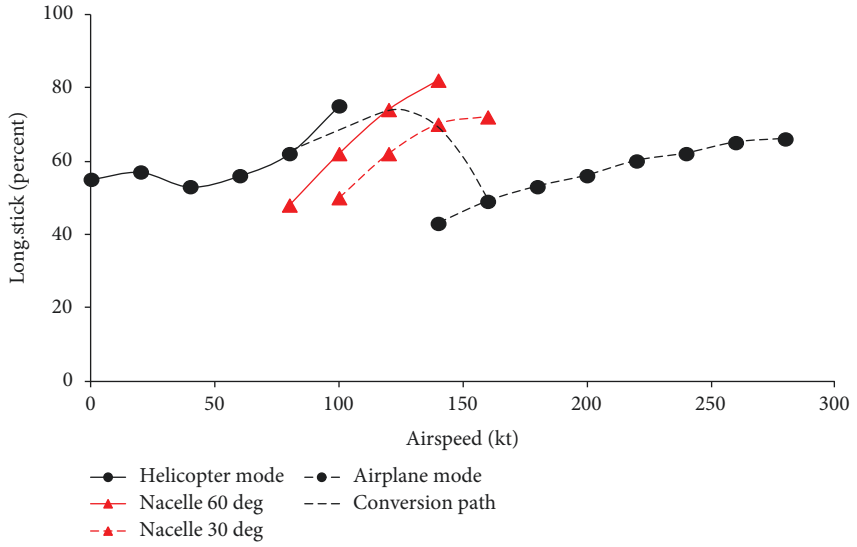

Figure 8: Longitudinal stick migration with respect to airspeed.

mode and passes through 120 knots in nacelle angle 60 deg and 140 knots in nacelle angle 30 deg, finally ends at 160 knots in airplane mode. The longitudinal stick is pushed forward with airspeed increasing before 120 knots. However, after 120 knots, longitudinal stick migrates after to gain airspeed. This results in apparent negative speed stability and mainly caused by the efficiency of the elevator that increases significantly with the flight speed. Reference [8] also has captured this feature.

Remark 1. In general, the speed stability for each flight mode is positive. However, when the tilt-rotor aircraft covert from helicopter mode to airplane mode, the longitudinal stick will migrate backward as the speed increases, showing a typical negative speed stability.

3. Dynamic Stability of the Tilt-Rotor Aircraft

There are 36 stability derivatives in the standard 6-DoF set [19]. In this section, a limited number of the more important tilt-rotor aircraft stability derivatives is discussed.

3.1. Translational Velocity Derivatives. Figure 9 presents the predicted heave damping derivatives Z_w of the tilt-rotor aircraft as a function of flight speed in different flight mode. The derivative Z_w represents the initial acceleration following an abrupt vertical gust [19]. For helicopter mode, the derivative

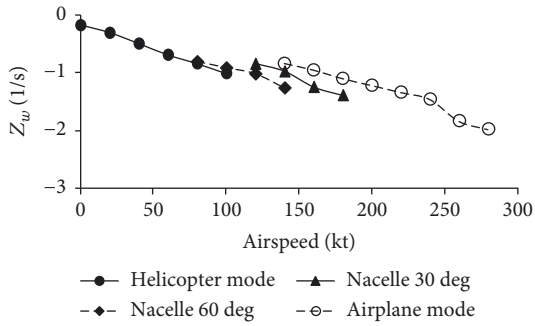

Figure 9: Variation of the derivative Z_w with forward speed.

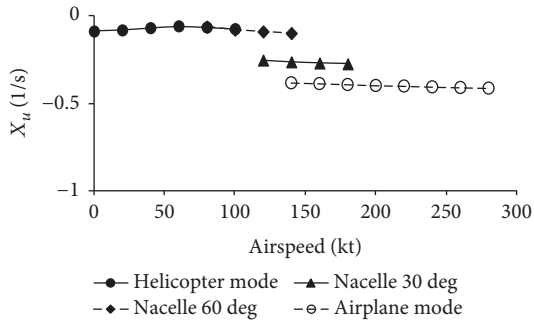

Figure 10: Variation of the derivative X_u with forward speed.

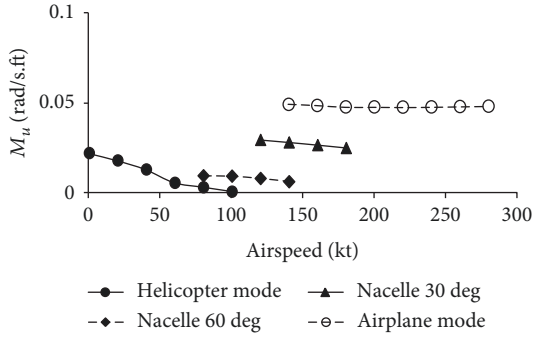

Figure 11: Variation of the derivative M_u with forward speed.

is determined mainly by the rotor in hover and low-speed flight and is given by

$$Z_w = -\frac{4a_0 A_b \rho(\Omega R)\lambda_i}{(16\lambda_i + a_0\sigma)m}. \quad (13)$$

In forward flight, the wing begins to contribute to the derivative and is given by

$$Z_w = -\frac{\rho a_0 \mu(\Omega R)A_b}{2m}\left(\frac{8}{8\mu + a_0\sigma}\right) - \frac{\rho a_w V A_w}{2m}. \quad (14)$$

For all flight mode, this derivative decreases with the increase of speed. It is worth noting that in the same flight speed (140 kt), the derivative of airplane mode is the largest because of the absence of the rotor contribution.

Figure 10 presents the drag damping derivatives X_u of the tilt-rotor aircraft as a function of flight speed in different flight

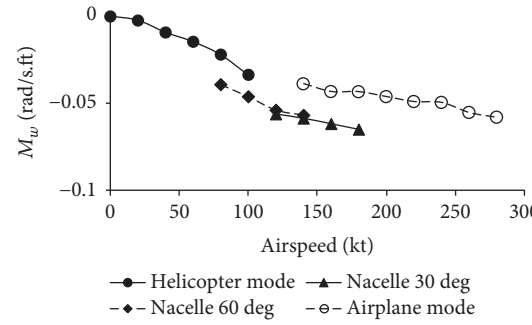

Figure 12: Variation of the derivative M_w with forward speed.

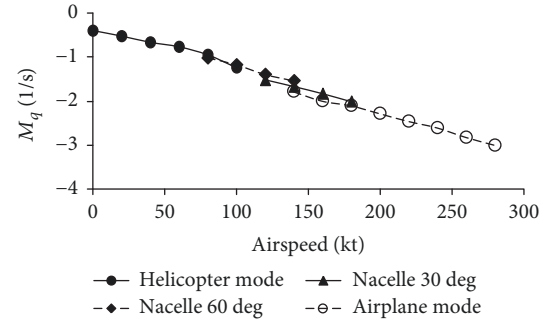

Figure 13: Variation of the derivative M_q with forward speed.

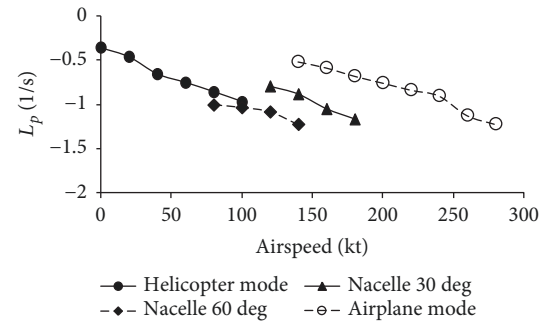

Figure 14: Variation of the derivative L_p with forward speed.

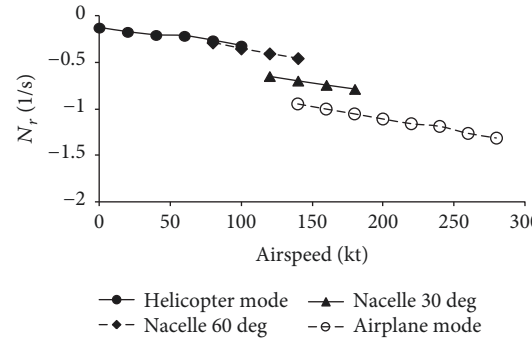

Figure 15: Variation of the derivative N_r with forward speed.

mode. This derivative is important as it is associated with the damping of the phugoid mode. In helicopter mode, this derivative is similar to a conventional helicopter, however, in airplane mode, in addition to the two propeller's contribution to X_u, a positive perturbation of u creating greater drag.

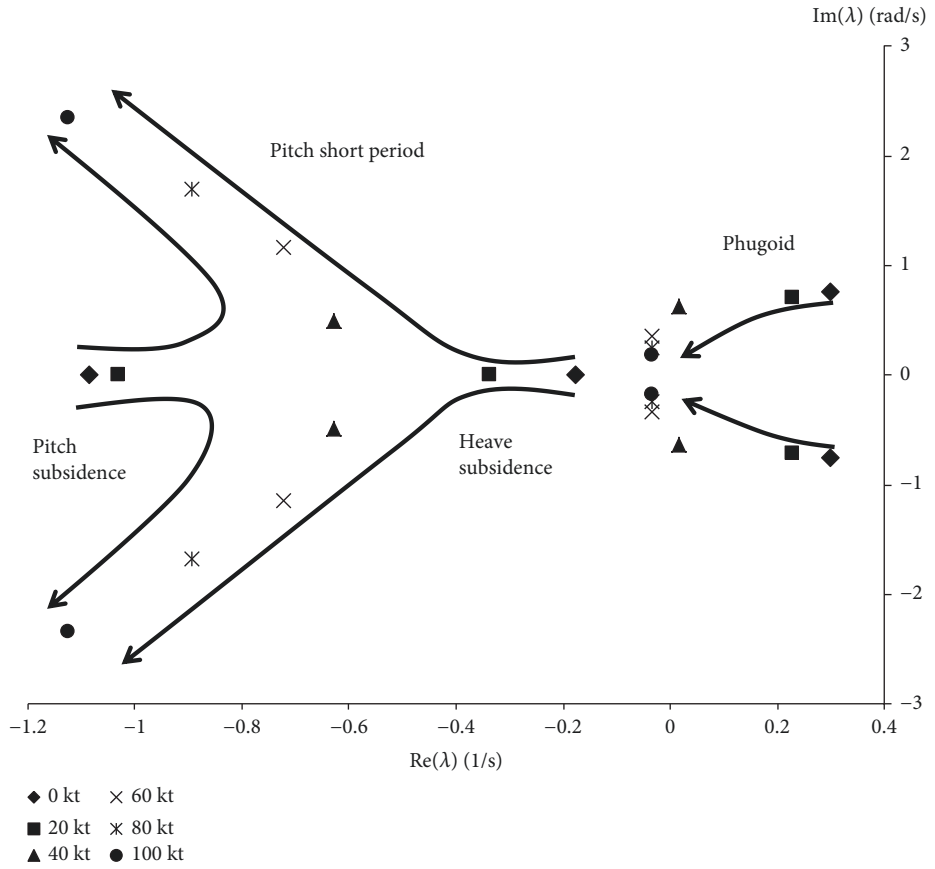

Figure 16: Longitudinal eigenvalue movement in helicopter mode.

Two important derivatives, M_u and M_w derivatives, the so-called speed and incidence static stability derivatives, have a major effect on longitudinal stability and hence handling qualities [19]. The estimated speed derivative can be seen in Figure 11. In all flight modes, the aircraft exhibits a positive stable response with the fuselage pitching up thereby decreasing the forward speed. This derivative has a significant effect on good handling qualities during forward flight [19], which will be discussed in the later section. As seen in Figure 11, this derivative is insensitive to airspeed except in helicopter mode.

Figure 12 presents the predicated incidence static stability derivatives of the tilt-rotor aircraft as a function of flight speed in different flight modes. This derivative, M_w, has a significant influence on the longitudinal short period motion modes [22]. The results here are negative throughout the speed range, and therefore it is steady. In helicopter mode, the rotor disc flaps back giving rise to a positive, destabilizing, pitching moment when encounters a positive perturbation in normal velocity. The fuselage and the wing provide destabilizing contributions to M_w as the main reason is that the center of gravity is after the aerodynamic center. However, for XV-15 tilt-rotor aircraft, the tailplane is large enough, so that it could provide a stabilizing enough contribution to M_w.

3.2. Angular Velocity Derivatives. Figure 13 shows the estimated values of the pitch damping derivatives M_q in all flight modes. The contribution of the stiffness of the rotor to the pitch damping derivative is given by [19]

$$\frac{\partial M_{\text{rotor}}}{\partial q} = -\frac{N_b S_\beta I_\beta \Omega}{I_{yy}} \left(1 + S_\beta \frac{\gamma}{16}\right), \quad S_\beta = \frac{8\left(\lambda_\beta^2 - 1\right)}{\gamma}. \tag{15}$$

The contribution of the spring stiffness is minor with a numerical value of -0.2. The main reason is that the rotor stiffness number is small with a numerical value of 0.0752. The tailplane is the main source contribution to this derivative, which changes in a linear manner with flight speed.

The roll damping derivative L_p reflects bandwidth and attitude quickness handling characteristics [19]. The estimated roll damping derivatives can be seen in Figure 14. For a conventional helicopter, this derivative is insensitive to airspeed [23]. In contrast, for XV-15 tilt-rotor aircraft, the roll damping derivative L_p is very much affected by the speed of the flight in all flight modes, as seen in Figure 14. In helicopter mode, the contribution to this derivative has two parts. One is due to the rotor lateral offset, and the other is due to the contribution of the wing. Both of these components provide a stabilizing rolling moment following a perturbation of the roll rate. In airplane mode, the wing is the main source of this derivative. In the same flight speed, the

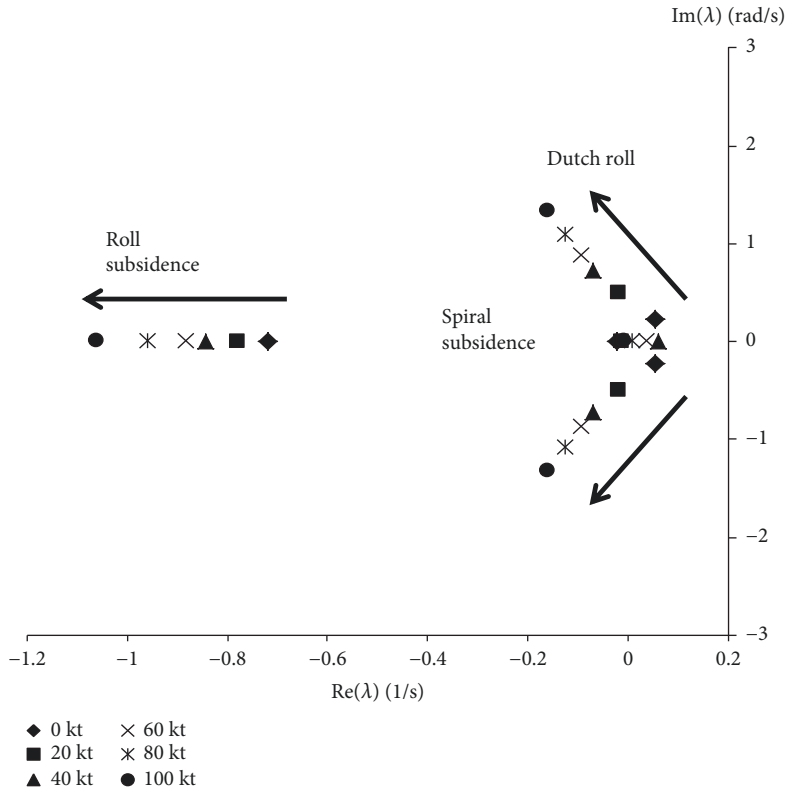

Figure 17: Lateral eigenvalue movement in helicopter mode.

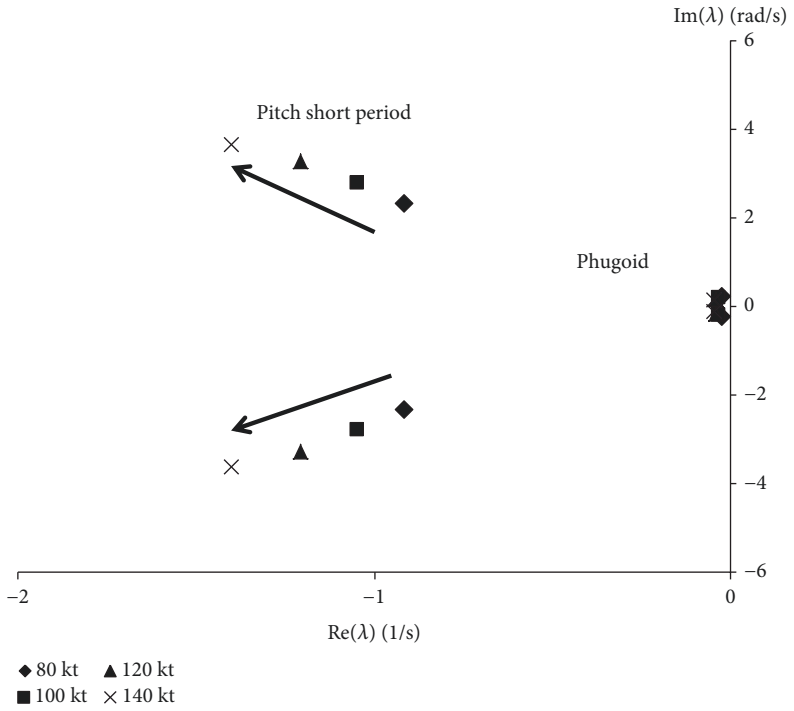

Figure 18: Longitudinal eigenvalue movement in nacelle 60 deg.

roll damping derivative of airplane mode is larger than the other flight modes. This is because the contribution of the rotor is diminishing.

Figure 15 presents the predicated yaw damping derivatives, N_r, of the tilt-rotor aircraft as a function of flight speed in different flight mode. The yaw damping derivative, N_r,

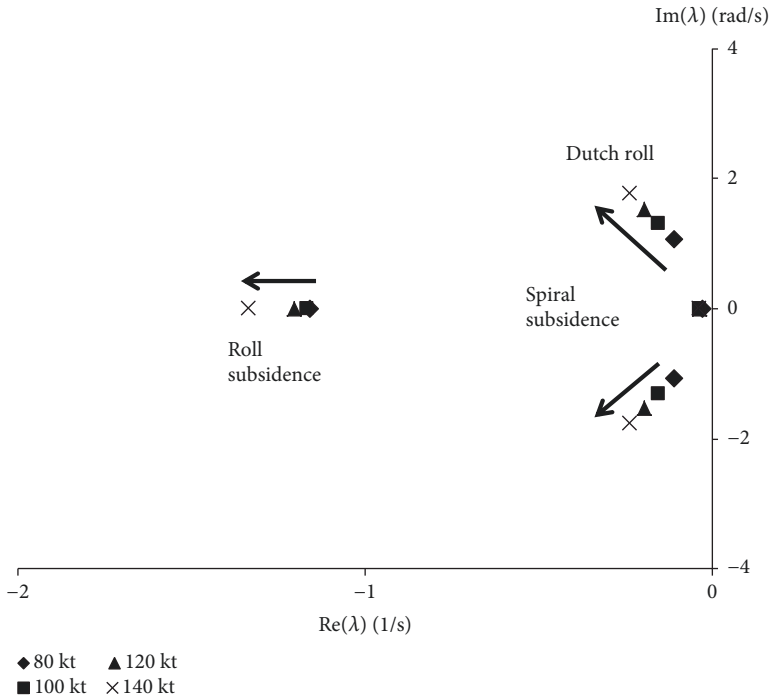

Figure 19: Lateral eigenvalue movement in nacelle 60 deg.

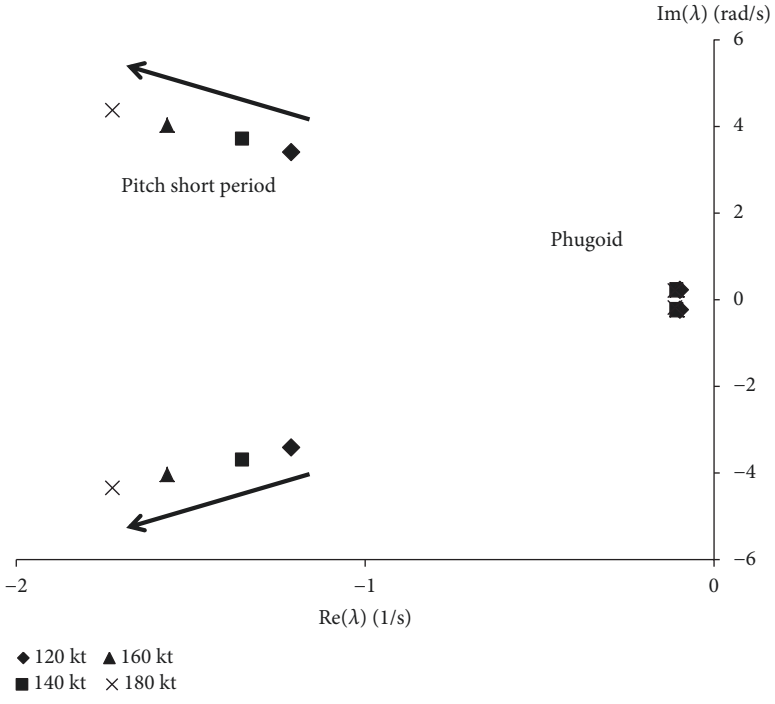

Figure 20: Longitudinal eigenvalue movement in nacelle 30 deg.

represents the yawing moment following a perturbation of yaw rate. A negative value represents stability [19, 23]. As the tilt-rotor aircraft does not need the tail rotor to balance the antitorque moment, as can be seen from Figure 15, the yaw damping derivative is not enough in low flight speed. In airplane mode, the two propellers provide a stabilizing contribution to the yaw damping derivative. This is why the aircraft mode has the maximum damping coefficient at the same flight speed in all flight modes. It indicates that the airplane mode has better Dutch roll damping and handling quality which will be explained in the following section of the paper.

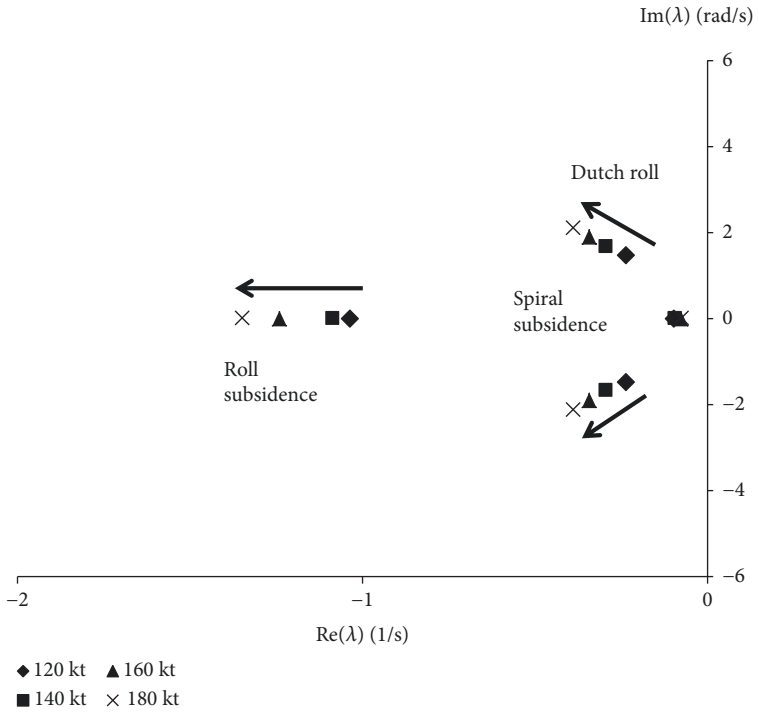

Figure 21: Lateral eigenvalue movement in nacelle 30 deg.

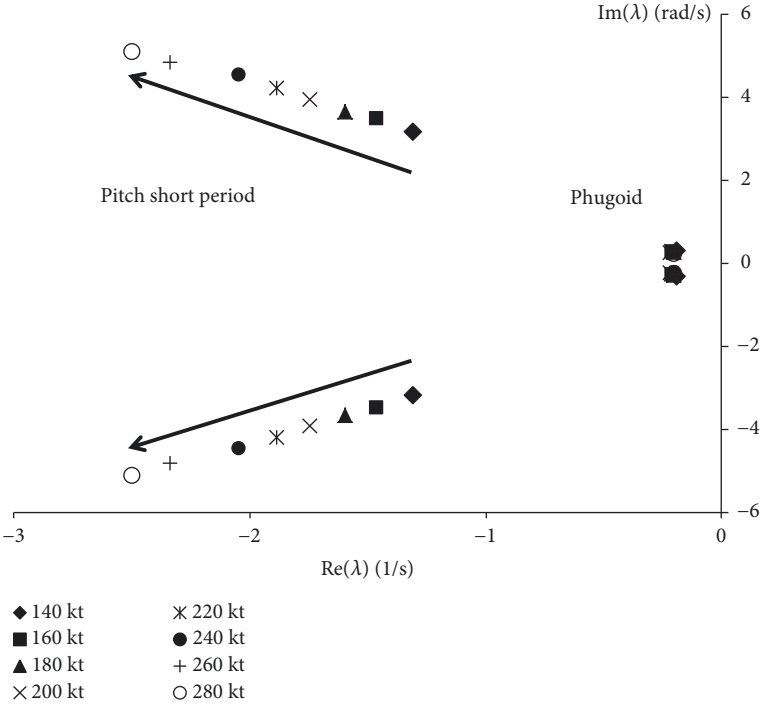

Figure 22: Longitudinal eigenvalue movement in airplane mode.

3.3. Natural Modes of Motion. In the previous section, we analyzed the stability derivatives of the XV-15 tilt-rotor aircraft and find out their main contribution sources. For small amplitude stability analysis, the tilt-rotor aircraft flight dynamics behavior can be described by a linear combination of natural modes.

Figures 16–23 illustrate the eigenvalue movements for helicopter mode, nacelle 60 deg, nacelle 30 deg, and airplane mode, respectively. For the short period modes, the eigenvalues of the short period modes are primarily influenced by the stability derivatives Z_w, M_q, and M_w. The approximate characteristic equation

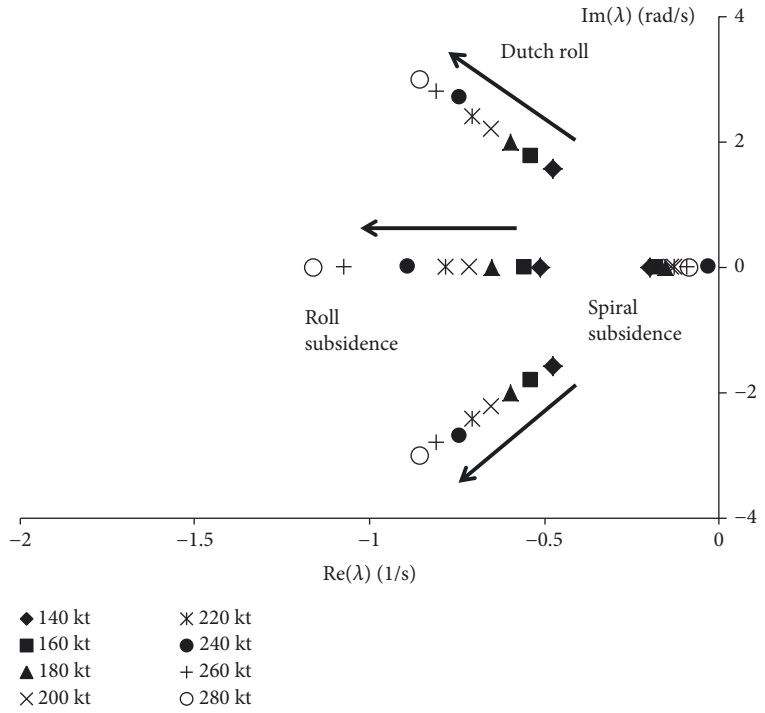

Figure 23: Lateral eigenvalue movement in airplane mode.

for predicting the stability of the short period mode is given by [19, 24]

$$\lambda_{sp}^2 - \left(Z_w + M_q\right)\lambda_{sp} + Z_w M_q - M_w\left(Z_q + U_e\right) = 0, \quad (16)$$

where the frequency and damping are given by the expressions

$$\begin{aligned} 2\zeta_{sp}\omega_{sp} &= -\left(Z_w + M_q\right), \\ \omega_{sp}^2 &= Z_w M_q - \left(Z_q + U_e\right)M_w. \end{aligned} \quad (17)$$

Blake et al. used a ground-based flight simulator and developed a relationship between pilot rating and longitudinal stability. They find out that the pilot rating will have a rapid degradation when the maneuver margin, $Z_w M_q - M_w(Z_q + U_e)$, approaches zero [22]. For XV-15 tilt-rotor aircraft, the maneuver margin is positive, which means the pitch short period modes are always stable. In all flight modes, the frequency increases as the flight speed increases while the damping is insensitive to flight speed.

As seen in Figure 16, the phugoid mode becomes more stable as speed increases and becomes a stable mode after 60 knots. The oscillatory frequency of phugoid mode is reduced due to the speed stability derivative M_u tending towards zero. In conversion and airplane mode, the phugoid modes meet the ADS-33E-PRF handling quality specification level 1 requirement (see Figures 18, 20 and 22).

The lateral/directional motion of tilt-rotor aircraft in forward flight is composed of a Dutch roll oscillation and two nonoscillating modes which are called roll and spiral modes [19]. The eigenvalue of the roll subsidence mode is approximately equal to the stability derivative L_p. While the roll motion of the tilt-rotor aircraft can be written in the first-order differential form of a rate response type:

$$\dot{p} - L_p p = L_{\delta_{\text{lat}}}\delta_{\text{lat}}, \quad (18)$$

where $L_{\delta_{\text{lat}}}$ is roll control sensitivity.

From the analysis in the previous section, we have known that the roll damping derivative L_p reflects bandwidth and attitude quickness handling characteristics. In all flight modes (see Figures 17, 19, 21 and 23), this eigenvalue moves to the left as the speed increases. Therefore, the bandwidth of the roll channel increases with speed. In conversion mode, the bandwidth will decrease as the rotors tilt forward in the same flight speed.

In terms of the Dutch roll mode, the frequency increases as the flight speed increases in all flight modes (see Figures 17, 19, 21 and 23). The damping of the Dutch roll mode is insensitive to flight speed; however, it is sensitive to flight mode. The damping of the Dutch roll mode in helicopter mode, nacelle 60 deg, nacelle 30 deg, and airplane mode is, respectively, 0.12, 0.13, 0.17, and 0.28, due to the contribution of the rotors. In airplane mode, the Dutch roll meets the ADS-33E-PRF handling quality specification level 1 requirement for all-other-MTEs.

Remark 2. The XV-15 tilt-rotor aircraft stability derivatives discussed above are all stable; however, the nacelle angle will

affect the contribution of the rotor and then affect the stability derivative magnitude and trend. In all flight modes, as flight speed increases, the natural modes become more stable. The damping of the pitch short period mode and the Dutch roll mode is insensitive to flight speed. In particular, the Dutch roll meets the ADS-33E-PRF handling quality specification level 1 requirement for all-other-MTEs for airplane mode.

4. Conclusions

In this paper, a nonlinear flight dynamics mode is developed, and then the dynamic stability of the tilt-rotor aircraft is assessed. The main conclusions from the current work are as follows:

(1) The XV-15 tilt-rotor flight dynamics model developed in this paper is proved to be valid

(2) The speed stability of the tilt-rotor aircraft is positive in certain flight modes; however, when the tilt-rotor aircraft covert from helicopter mode to airplane mode, it is apparent typical negative speed stability

(3) The stability derivatives in all flight modes are stable, while the nacelle angle could affect their magnitude and trend. For example, the contribution of the rotors to the heave damping derivative Z_w in helicopter mode becomes to the drag damping derivative X_u in airplane mode

(4) The natural modes become more stable with flight speed increases. The damping of the pitch short period mode and the Dutch roll mode is insensitive to flight speed, while they are sensitive to nacelle angle

Nomenclature

a_w: Wing lift cure slope (1/rad)
a_0: Rotor blade lift cure slope (1/rad)
g: Acceleration due to gravity (m/s^2)
i_n: Mast angle (rad)
m: Aircraft mass (kg)
u, v, w: Translational velocities (m/s)
p, q, r: Angular velocities (rad/s)
v_i: Induced velocity (m/s)
t: Time (s)
$\bar{r}$: Blade radial coordinate nondimensionalized on R
r: Blade radial coordinate (m)
$\mathbf{A}$: System matrix
A_b: Blade area (m^2)
A_w: Wing area (m^2)
$\mathbf{B}$: Control matrix
I_β: Flap moment of inertia (kg·m^2)
I_{yy}: Pitch moment of inertia (kg·m^2)
K_P: Pitch-flap coupling ratio, $\triangleq \tan \delta_3$
K_β: Flapping hinge restraint (Nm/rad)
L_p: Roll damping derivative (1/s)
L_v: Dihedral effect (rad/s·m)
M_u: Speed static stability derivative (rad/s·m)
M_w: Incidence static stability derivative (rad/s·m)
N_r: Yaw damping derivative (1/s)
N_v: Weathercock stability (rad/s·m)
N_b: Number of blades
R: Rotor radius (m)
S_β: Stiffness number
U_e: Trim body x-axis velocity (m/s)
X_u: Drag damping derivative (1/s)
Y_v: Side force damping derivative (1/s)
Z_w: Heave damping derivative (1/s)
V: Forward flight velocity (m/s)
ϕ, θ, ψ: Euler angles (rad)
α_n^m, β_n^m: Induced inflow expansion coefficients
β: Rotor flap angle (rad)
β_p: Blade precone angle (rad)
δ_3: Pitch-flap coupling angle (rad)
δ_{coll}: Collective stick input (cm)
δ_{lat}: Lateral stick input (cm)
δ_{long}: Longitudinal stick input (cm)
δ_{ped}: Pedal deflection (cm)
θ_0: Blade-root collective pitch (rad)
θ_b: Blade pitch angle (rad)
θ_t: Blade twist angle (rad)
θ_{1c}: Lateral cyclic pitch (rad)
θ_{1s}: Longitudinal cyclic pitch (rad)
$\phi_n^m(\bar{r})$: Radial expansion shape function
μ: Advance ratio
δ_3: Pitch-flap coupling angle
γ: Lock number
λ_i: Rotor inflow
λ_{sp}: Pitch short period eigenvalue
λ_β: Flap frequency ratio
ς_{sp}: Pitch short period damping factor
ω_{sp}: Pitch short period frequency (rad/s)
ς_{dr}: Dutch roll damping factor
ω_{dr}: Dutch roll frequency (rad/s)
σ: Rotor solidity
Ω: Rotor angular velocity (rad/s)
ρ: Air density (kg/m^3)
Ψ: Azimuthal location of reference blade (rad).

Data Availability

The data used to support the findings of this study are available from the corresponding author upon request.

Conflicts of Interest

The authors declare that there is no conflict of interest regarding the publication of this paper.

Authors' Contributions

Ke Lu and Chunsheng Liu designed the research and wrote the paper; Chunhua Li and Renliang Chen helped perform the analysis with constructive discussions.

Acknowledgments

This work was supported by the Aeronautical Science Foundation of China (Grant Nos. 20175752045; 2016ZA02001) and the National Natural Science Foundation of China (Grant No. 11672128).

References

[1] J. Leishman, *Principles of Helicopter Aerodynamics*, Cambridge University Press, 2nd edition, 2006.

[2] M. D. Masiel and D. J. Giulianetti, "The history of the XV-15 tilt rotor aircraft: from concept to flight," Tech. Rep. NASA SP-2000-4517, 2000.

[3] S. W. Ferguson, "A mathematical model for real time flight simulation of a generic tilt-rotor aircraft," Tech. Rep. NASA CR-166536, 1988.

[4] R. L. Marr, K. W. Sambell, and G. T. Neal, "V/STOL tilt rotor study-volume VI, hover, low speed and conversion tests of a tilt Rotor aeroelastic model," Tech. Rep. NASA-CR-114615, 1973.

[5] J. Schillings John, B. J. Roberts, T. L. Wood, and K. G. Wernicke, "Maneuver performance comparison between the XV-15 and an advanced tiltrotor design," *Journal of the American Helicopter Society*, vol. 35, no. 2, pp. 4–14, 1990.

[6] M. B. Tischler, "Identification and verification of frequency domain models for XV-15 tilt-rotor aircraft dynamics," Tech. Rep. NASA-TM-86009, 1984.

[7] M. B. Tischler, "Frequency-response identification of XV-15 tilt-rotor aircraft dynamics," Tech. Rep. NASA-TM-89428, 1987.

[8] K. M. Kleinhesselink, *Stability and control modeling of tilt-rotor aircraft, [M.S. thesis]*, University of Maryland, 2007.

[9] C. W. Acree Jr., H. Yeo, and J. Sinsay, "Performance optimization of the NASA large civil tilt-rotor," Tech. Rep. NASA/TM-2008-215359, 2008.

[10] O. Juhasz, R. Celi, C. M. Ivler, M. B. Tischler, and T. Berger, "Flight dynamic simulation modeling of large flexible tilt-rotor aircraft," in *American Helicopter Society 68th Annual Forum*, Fort Worth, TX, USA, May 2012.

[11] C. Malpica, W. A. Decker, C. R. Theodore, C. L. Blanken, and T. Berger, "An investigation of large tilt-rotor short term attitude response handling qualities requirements in hover," in *American Helicopter Society 66th Annual Forum*, Phoenix, AZ, uSA, May 2010.

[12] C. Malpica, C. R. Theodore, W. A. Decker, B. Lawrence, and C. L. Blanken, "An investigation of large tilt-rotor hover and low speed handling qualities," in *American Helicopter Society 67th Annual Forum*, Virginia Beach, VA, USA, May 2011.

[13] B. Lawrence, C. Malpica, C. R. Theodore, W. A. Decker, and J. E. Lindsey, "Flight dynamics aspects of a large civil tilt-rotor simulation using translational rate command," in *American Helicopter Society 67th Annual Forum*, Virginia Beach, VA, USA, May 2011.

[14] W. Johnson, *Rotorcraft Aeromechanics*, Cambridge University Press, 1st ed. edition, 2013.

[15] D. A. Peters and H. Chengjian, "Finite state induced flow models part II: three-dimensional rotor disk," *Journal of Aircraft*, vol. 32, no. 2, pp. 323–333, 1995.

[16] C. He, *Development and application of a generalized dynamic wake theory for lifting rotors, [Ph.D. thesis]*, Georgia Institue of Technology, 1989.

[17] E. B. Carlson and Y. J. Zhao, "Prediction of tiltrotor height-velocity diagrams using optimal control theory," *Journal of Aircraft*, vol. 40, no. 5, pp. 896–905, 2003.

[18] L. Marr Roger and W. E. B. Roderick, "Handling qualities evaluation of the XV-15 tilt rotor aircraft," *Journal of the American Helicopter Society*, vol. 20, no. 2, pp. 23–33, 1975.

[19] G. D. Padfield, *Helicopter Flight Dynamics: The Theory and Application of Flying Qualities and Simulation Modelling, Second Edition*, Blackwell Pub, Oxford, 2007.

[20] C. Yihua, Q. Qi, and D. Zhang, "Flight dynamic characteristics of tiltrotor aircraft slung-load system," *Journal of Aircraft*, vol. 54, no. 3, pp. 1221–1228, 2017.

[21] Anon, "Handling qualities requirements for military rotorcraft. Aeronautical design standard ADS-33E-PRF," United States Army Aviation and Troop Command, 2000.

[22] B. B. Blake, I. B. Alansky, and B. V. Co, "Stability and control of the YUH-61A," *Journal of the American Helicopter Society*, vol. 22, no. 4, pp. 2–9, 1977.

[23] K. Ferguson and D. Thomson, "Examining the stability derivatives of a compound helicopter," *The Aeronautical Journal*, vol. 121, no. 1235, pp. 1–20, 2017.

[24] F. Kevin and D. Thomson, "Flight dynamics investigation of compound helicopter configurations," *Journal of Aircraft*, vol. 52, no. 1, pp. 156–167, 2015.